Single-Baseline Polarimetric SAR Interferometry

Konstantinos P. Papathanassiou and Shane R. Cloude

***Abstract*—The objective of this paper is to examine the application of single-baseline polarimetric SAR interferometry to the remote sensing and measurement of structure over forested terrain. For this, a polarimetric coherent scattering model for vegetation cover suitable for the estimation of forest parameters from interferometric observables is introduced, discussed and validated. Based on this model, an inversion algorithm which allows the estimation of forest parameters such as tree height, average extinction, and underlying topography from single-baseline fully polarimetric interferometric data is addressed. The performance of the inversion algorithm is demonstrated using fully polarimetric single baseline experimental data acquired by DLR's E-SAR system at L-band.**

***Index Terms*—Forest parameter inversion, polarimetric interferometry, radar polarimetry, synthetic aperture radar (SAR) interferometry.**

I. Introduction

SAR interferometry is an established technique for the estimation of the height location of scatterers through the phase difference in images acquired from spatially separated locations at either end of a baseline [1]. The high sensitivity of the interferometric phase and coherence to vegetation height and density variations makes the estimation of forest parameters from interferometric observables a challenge [2]–[5]. A common problem for all estimation techniques arises from the complexity of the scattering process, which does not provide easy separability of the physical forest parameters in terms of the interferometric observables. This prevents a straightforward parameter estimation and requires inversion of a scattering model which relates the interferometric observables to physical parameters of the scattering process.

The choice of the scattering model is essential for the performance of any inversion algorithm. On the one hand, the model must be correct, i.e., it must contain enough physical structure to interpret and predict the behavior of the observables. On the other hand it must be simple enough in terms of parameters in order to be determinable with a limited number of observables. Complex scattering models lead to underestimated inversion problems, as in general, the collection of an adequate number of observables is problematic for conventional air or spaceborne SAR systems. Such inversion problems can be solved unambiguously only under simplifying assumptions or *a priori* information and have therefore a constrained applicability.

One very promising way to extend the interferometric observation space is through the introduction of polarization. Scattering polarimetry is sensitive to the shape, orientation, and dielectric properties of scatterers. This allows the identification and separation of scattering mechanisms of natural media employing differences in the polarization signature for purposes of classification and parameter estimation [6]. In polarimetric interferometry both techniques are coherently used to provide combined sensitivity to the vertical distribution of scattering mechanisms [7]. Hence, it becomes possible to investigate the three-dimensional (3-D) structure of vegetation cover using only a single-frequency polarimetric radar sensor. In [7], a first-order estimator for tree height was introduced based on the phase difference between interferograms formed using different polarizations. While the proposed technique was simple in implementation, it leads to underestimated tree heights and its applicability is limited due to its assumptions about the presence of orthogonal deterministic scattering mechanisms. In this paper, we propose a generalization of the ideas presented in [7] and address a more sophisticated model-based inversion algorithm for forest parameter estimation.

For this, a review of the basic concepts of polarimetric interferometry is given in Section II. Section III introduces a coherent scattering model suitable for the description of interferometric and polarimetric behavior of forested terrain. The influence of ground scattering and polarization on the interferometric behavior of the model is discussed. Finally, the validity of the model is demonstrated using experimental data. Based on this model, in Section IV, we propose an inversion algorithm for forest height, average forest extinction, and underlying topography from single baseline fully polarimetric interferometric data. Further, we evaluate the influence of the selected polarizations on the performance of the inversion algorithm and demonstrate the potential of the proposed technique against ground measurements.

II. Polarimetric Interferometry

A monostatic, fully polarimetric interferometric system measures for each resolution element in the scene from two slightly different look angles, two scattering matrices $[\,S_1\,]$, and $[\,S_2\,]$. Assuming reciprocal scattering, the 3-D Pauli-scattering vectors $\vec{k}_1$ and $\vec{k}_2$ are then given by [6]

$$\vec{k}_1 = \frac{1}{\sqrt{2}}\left[\, S_{1_{HH}} + S_{1_{VV}},\ S_{1_{HH}} - S_{1_{VV}},\ 2S_{1_{HV}} \,\right]^T \quad (1)$$

$$\vec{k}_2 = \frac{1}{\sqrt{2}}\left[\, S_{2_{HH}} + S_{2_{VV}},\ S_{2_{HH}} - S_{2_{VV}},\ 2S_{2_{HV}} \,\right]^T. \quad (2)$$

The complete information measured by the SAR system can be represented in form of three 3×3 complex matrices $[T_{11}]$, $[T_{22}]$, and $[\,\Omega_{12}\,]$ formed using the outer products of $\vec{k}_1$ and $\vec{k}_2$ as

$$[T_{11}] := \langle \vec{k}_1 \cdot \vec{k}_1^{\dagger} \rangle,\ [T_{22}] := \langle \vec{k}_2 \cdot \vec{k}_2^{\dagger} \rangle,\ [\Omega_{12}] := \langle \vec{k}_1 \cdot \vec{k}_2^{\dagger} \rangle. \quad (3)$$

Manuscript received September 29, 2000; revised August 8, 2001. This work was supported by the EC-TMR Polarimetry Network ERB-FMRX-CT98–0211 and ONR-NICOP N00014–97-C-0281 Projects.

K. P. Papathanassiou is with the German Aerospace Center (DLR), D-82234 Wessling, Germany.

S. R. Cloude is with AEL Consultants, Cupar KY15 5AA, U.K.

Publisher Item Identifier S 0196-2892(01)09892-8.

$[\,T_{11}\,]$ and $[\,T_{22}\,]$ are the conventional hermitian coherency matrices [6] that describe the polarimetric properties for each image separately, while $[\,\Omega_{12}\,]$ is a 3×3 nonhermitian complex matrix that contains polarimetric and interferometric information.

Introducing two unitary complex vectors $\vec{w}_1$ and $\vec{w}_2$, which may be interpreted as generalized scattering mechanisms [7], we are able to generate two complex scalar images i_1 and i_2 by projecting the scattering vectors $\vec{k}_1$ and $\vec{k}_2$ onto $\vec{w}_1$ and $\vec{w}_2$, respectively, as

$$i_1 = \vec{w}_1^{\,\dagger}\cdot\vec{k}_1 \quad \text{and} \quad i_2 = \vec{w}_2^{\,\dagger}\cdot\vec{k}_2. \tag{4}$$

The interferogram related to the scattering mechanisms $\vec{w}_1$ and $\vec{w}_2$ is then given by

$$i_1 i_2^* = (\vec{w}_1^{\,\dagger}\cdot\vec{k}_1)(\vec{w}_2^{\,\dagger}\cdot\vec{k}_2)^{\,\dagger} = \vec{w}_1^{\,\dagger}[\,\Omega_{12}\,]\,\vec{w}_2 \tag{5}$$

and the corresponding interferometric phase follows as:

$$\phi = \arg\{i_1 i_2^*\} = \arg\{\vec{w}_1^{\,\dagger}[\,\Omega_{12}\,]\,\vec{w}_2\}. \tag{6}$$

Finally, using (4)–(5), a general expression for the complex interferometric coherence for an arbitrary choice of scattering mechanisms $\vec{w}_1$ and $\vec{w}_2$ may be derived as [7]

$$\tilde{\gamma}(\vec{w}_1,\vec{w}_2) = \frac{\langle \vec{w}_1^{\,\dagger}[\,\Omega_{12}\,]\,\vec{w}_2\rangle}{\sqrt{\langle \vec{w}_1^{\,\dagger}[\,T_{11}\,]\,\vec{w}_1\rangle\langle \vec{w}_2^{\,\dagger}[\,T_{22}\,]\,\vec{w}_2\rangle}} \tag{7}$$

with $0 \le |\tilde{\gamma}| \le 1$. For convenience, we will distinguish in the following between the conventional coherence coefficient γ and the complex coherence value $\tilde{\gamma} = \gamma\exp(i\phi)$, which includes additionally the interferometric phase.

As demonstrated in [7], the interferometric coherence has a strong dependency on the polarizations used to form the interferogram. The evaluation of the scattering mechanisms that provide the highest possible interferometric coherence leads to two 3×3 complex eigenvalue problems with common eigenvalues ν_j

$$[\,T_{22}\,]^{-1}[\,\Omega_{12}\,]^{\,\dagger}[\,T_{11}\,]^{-1}[\,\Omega_{12}\,]\vec{w}_{2j} = \nu_j\vec{w}_{2j} \tag{8}$$

$$[\,T_{11}\,]^{-1}[\,\Omega_{12}\,][\,T_{22}\,]^{-1}[\,\Omega_{12}\,]^{\,\dagger}\vec{w}_{1j} = \nu_j\vec{w}_{1j}. \tag{9}$$

The solution of (8)–(9) yields three pairs (one for each image) of eigenvectors $\{\vec{w}_{1j},\vec{w}_{2j}\}$, with $j=1,2,3$ representing the optimum scattering mechanisms. The projection of the scattering vectors $\vec{k}_1$ and $\vec{k}_2$ onto $\vec{w}_{1j}$ and $\vec{w}_{2j}$ leads to the two optimized scalar complex images i_{1j} and i_{2j}, which are used for the interferogram formation

$$i_{1j} i_{2j}^* = (\vec{w}_{1j}^{\,\dagger}\cdot\vec{k}_1)(\vec{w}_{2j}^{\,\dagger}\cdot\vec{k}_2)^{\,\dagger} = \vec{w}_{1j}^{\,\dagger}\,[\,\Omega_{12}\,]\,\vec{w}_{2j}. \tag{10}$$

We obtain the complex coherence values using the square roots of the real eigenvalues ν_j and the corresponding interferometric phases as

$$\tilde{\gamma}_j = \sqrt{\nu_j}\,\exp\big(i\arg\{\vec{w}_{1j}^{\,\dagger}\,[\,\Omega_{12}\,]\,\vec{w}_{2j}\}\big). \tag{11}$$

In this paper, we are concerned with the physical interpretation of the optimum scattering mechanisms and the way in which they can be used for the inversion of forest parameters from SAR data.

III. Scattering Model

For the extraction of physical parameters from interferometric data, a coherent model of the scattering process which relates the measurables to the desired parameters is required [4], [5], [8], [9]. In the case of forest scattering at L-band, a realistic scattering model has to consider both the vegetation layer and ground interactions. A most simple model to describe such a scenario is the random volume over ground scattering model. Accordingly, the vegetation layer is modeled as a layer of thickness h_V containing a volume with randomly oriented particles and scattering amplitude per unit volume m_V, as shown schematically in Fig. 1. This random volume is located over a ground scatterer positioned at $z = z_0$ with scattering amplitude m_G. The ground is seen through the vegetation layer by an interferometric system operating at wavelength λ with physical baseline B under a mean incident angle θ_0 at range R. In this case, the complex interferometric coherence $\tilde{\gamma}$, after range spectral filtering, may by written as [4], [5], [8]

$$\tilde{\gamma}(\vec{w}) = \exp(i\phi_0)\frac{\tilde{\gamma}_V + m(\vec{w})}{1+m(\vec{w})} \tag{12}$$

where ϕ_0 is the phase related to the ground topography and m the effective ground-to-volume amplitude ratio accounting for the attenuation through the volume

$$m(\vec{w}) = \frac{m_G(\vec{w})}{m_V(\vec{w})}\exp\left(-\frac{2\sigma h_V}{\cos\theta_0}\right). \tag{13}$$

$\tilde{\gamma}_V$ denotes the complex coherence for the volume alone, which depends on the extinction coefficient σ for the random volume, and its thickness h_V as [4], [5]

$$\tilde{\gamma}_V = \frac{I}{I_0} \quad \begin{cases} I = \int_0^{h_V}\exp\left(\frac{2\sigma z'}{\cos\theta_0}\right)\exp(i\kappa_z z')\,dz' \\ I_0 = \int_0^{h_V}\exp\left(\frac{2\sigma z'}{\cos\theta_0}\right)dz' \end{cases} \tag{14}$$

The extinction coefficient σ corresponds to a mean extinction value for the vegetation layer, and is a function of the density of scatterers in the volume and their dielectric constant. κ_z is the effective vertical interferometric wavenumber after range spectral filtering, which depends on the imaging geometry and the radar wavelength

$$\kappa_z = \frac{\kappa\Delta\theta}{\sin\theta_0} \quad \kappa = \frac{4\pi}{\lambda}. \tag{15}$$

$\Delta\theta$ is the incidence angle difference induced by the baseline B. According to (12), the effective scattering center is located above the ground at a height which depends on the ground-to-volume amplitude ratio m as well as the attenuation length of the vegetation layer.

Equations (12)–(15) address the coherent random volume over a ground scattering problem as a four parameter problem regarding: 1) the volume thickness h_V (in meters); 2) the volume extinction coefficient σ (in dB/m); 3) the effective ground-to-volume amplitude ratio m; and 4) the phase ϕ_0

Fig. 1. Schematic representation of the random volume over ground scattering model.

(in radians) related to the underlying topography. Hence, even this simple model leads to an underestimated inversion problem for a single-channel single-baseline interferometric system. Consequently, in the absence of *a priori* assumptions, multiparameter interferometric configurations are needed for the estimation of forest parameters.

A. Effect of Ground on the Interferometric Coherence

Because of their different height distributions, volume and ground scattering have a significantly different interferometric behavior. In the volume, the scattering particles are distributed over the height h_V, and the effective phase center results from the coherent integration of their phasors over h_V. In contrast, the ground is characterized by a localized scattering phase center and the contributions of each elementary surface scattering element are added in phase with each other. Therefore, the ground scattering contribution affects the location of the effective scattering center (and consequently the interferometric coherence) in a very sensitive way, even if its backscattering amplitude is much smaller than that from the volume.

Fig. 2 shows on the left hand side the dependency of the interferometric coherence of the volume layer alone $|\tilde{\gamma}_V|$ on the extinction coefficient σ and the height h_V according to (14) for the case of an L-band interferometric system ($\lambda = 0.24$ m) operating at a height of 3220 m with a baseline of $B = 25$ m and incident angle $\theta_0 = 30°$. It demonstrates clearly the height-extinction ambiguity in the interpretation of the interferometric coherence. High vegetation with a high extinction coefficient may be characterized by the same coherence as tall vegetation with a lower extinction coefficient, as both cases may have the same attenuation length [3], [4]. Hence, the interferometric coherence alone is not sufficient for unambiguous extraction of vegetation height from interferometric data.

The influence of ground scattering on the interferometric coherence $|\tilde{\gamma}|$ is demonstrated on the right hand side of Fig. 2, where the variation of $|\tilde{\gamma}|$ as a function of the ground-to-volume amplitude ratio m and the height h_V for a fixed extinction $\sigma = 0.2$ dB/m , in terms of (12), is shown. As the ground component increases from zero, the effective phase center moves toward the ground, increasing the effective height distribution of the scatterers and reducing the interferometric coherence. However, as the ground amplitude becomes on the order of the volume amplitude the interferometric coherence increases with increasing ground component, as a consequence of the presence of a localized scattering center. The influence of the ground is especially critical for $10^{-1} < m < 1$, where an increase of m of the order of few percent can occasionally (depending on the actual h_V and σ values) increase or decrease considerably the interferometric coherence, leading to a biased estimation of h_V and σ. Consequently, the accurate estimation of the ground-to-volume amplitude ratio is a key element in the inversion of h_V and σ from interferometric data especially at frequencies or polarizations which are characterized by a low ground-to-volume amplitude ratio.

B. Effect of Polarization on the Interferometric Coherence

In this section, we investigate the influence of polarization on the interferometric behavior of the random volume over ground scattering model. For this, we consider first the case of an isolated random volume. Random volumes are characterized by a diagonal polarimetric coherency matrix

$$[T_V] = m_V \begin{bmatrix} 1 & 0 & 0 \\ 0 & f & 0 \\ 0 & 0 & f \end{bmatrix} \tag{16}$$

where f ranges between 0 and 0.5 depending only on the shape and dielectric constant of the particles in the volume [10]. In the case where the particles are spheres, $f = 0$, while at the other extreme, when the volume particles are dipoles, $f = 0.5$. From (16), it follows that in the general case of nonspherical particles, the volume is present in all polarization channels. Furthermore, the wave propagation through the random volume is scalar, i.e., polarization independent. Therefore, polarization has no influence on the location of the scattering center and consequently on the interferometric coherence $\tilde{\gamma}_V$ apart from the amount of backscattered intensity. Assuming a sufficiently high backscattered signal in all polarizations, this leads to interferograms with the same coherence $\tilde{\gamma}_V$. The interferometric coherence, for given h_V and σ, depends only on the vertical wavenumber κ_z. In this special case, polarimetric interferometry does not provide any additional information over single channel interferometry. Single polarization multibaseline approaches may be used for the estimation of h_V and σ based on its dependency on κ_z [4].

The situation changes dramatically with the introduction of the ground in the scattering scenario. The fact that the ground has a strongly polarization dependent behavior combined with the sensitive way in which even small ground scattering contributions affect the interferometric coherence makes polarimetric interferometry an important technique for the quantitative study of vegetation layers. The sensitivity of the interferometric coherence to even a small component of ground scattering forces consideration of a multicomponent depolarizing ground scatterer [11], [12]. The covariance matrix of such a ground scatterer is, under the assumption of reflection symmetry, of the form

$$[T_G] = \begin{bmatrix} t_{11} & t_{12} & 0 \\ t_{12}^* & t_{22} & 0 \\ 0 & 0 & t_{33} \end{bmatrix}. \tag{17}$$

From (17) it follows that, similar to the volume, the ground is present in all polarizations and cannot be removed by choosing an appropriate polarization. Nevertheless, the main difference is

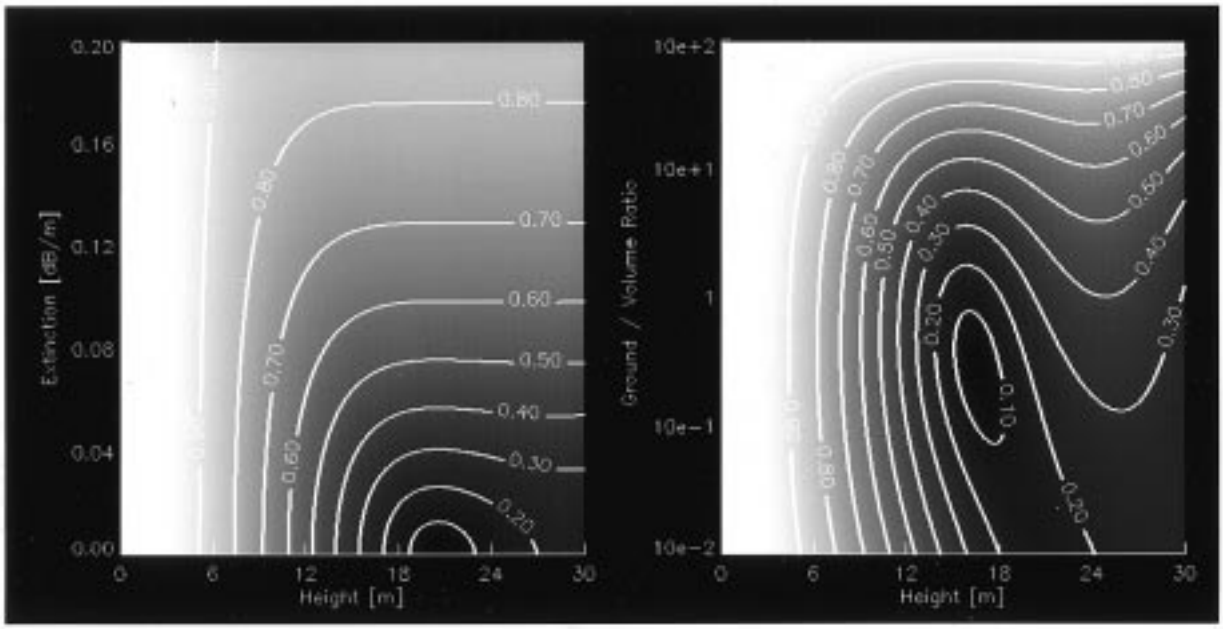

Fig. 2. Modeled interferometric coherence $|\tilde{\gamma}|$. (Left) As a function of volume height h_V and extinction coefficient σ ($m = 0$). (Right) As a function of volume height h_V and ground-to-volume amplitude m ($\sigma = 0.2$ dB/m).

that the amplitude of the ground varies much more strongly with polarization than the corresponding volume amplitude. For surfaces, the variation can be up to 25 dB (depending on the surface roughness), while typical variations of the volume scatterer are on the order of 5–10 dB (depending on the shape of the volume particles).

C. Experimental Observations

The experimental data used in the following are fully polarimetric repeat-pass interferometric L-band data of the Oberpfaffenhofen, Germany, test site, acquired by the airborne experimental SAR system operated by the German Aerospace Center (DLR), Oberpfaffenhofen, Germany, in the frame of a multibaseline experiment in May 1998 [13]. As the data were acquired in a repeat pass mode with a temporal baseline of about 10 min, temporal decorrelation effects have to be considered. In order to obtain an estimate of the amount of temporal decorrelation, a zero baseline with respect to the first track has been flown at the end of the experiment. The high coherence ($|\tilde{\gamma}| \approx 1$) of this zero baseline interferogram allows us to neglect the effect of temporal decorrelation for the interpretation of this particular data set [13].

In Fig. 3, the $|S_{HV}|$ image of the test site is shown. The influence of polarization on the interferometric coherence of experimental data is demonstrated in Fig. 4, where the coherence maps of the $S_{1_{HH}} S^*_{2_{HH}}$, $S_{1_{HV}} S^*_{2_{HV}}$ and $S_{1_{VV}} S^*_{2_{VV}}$ interferograms for two baselines $B = 15$ m (top), and $B = 25$ m (bottom) are shown. The scaling from black to white corresponds to the coherence range from 0 to 1. According to the considerations outlined in A and B, the observed polarization dependency of the coherence values over the forested areas validates the presence of ground scattering. Further, the appearance of three discriminated coherence values indicates at least two different ground-to-volume amplitude ratios in the different polarizations. This confirms the assumption of a multicomponent ground scattering process. As the coherence for a ground scatterer is independent of baseline because of its isolated scattering center, any baseline variation of the observed coherence is induced by a volume scattering component. One can see that not only the S_{HV} channel but also the S_{HH} and S_{VV} channels are affected by significant volume scattering contributions.

Fig. 3. L-band $|S_{HV}|$ image of the Oberpfaffenhofen test site.

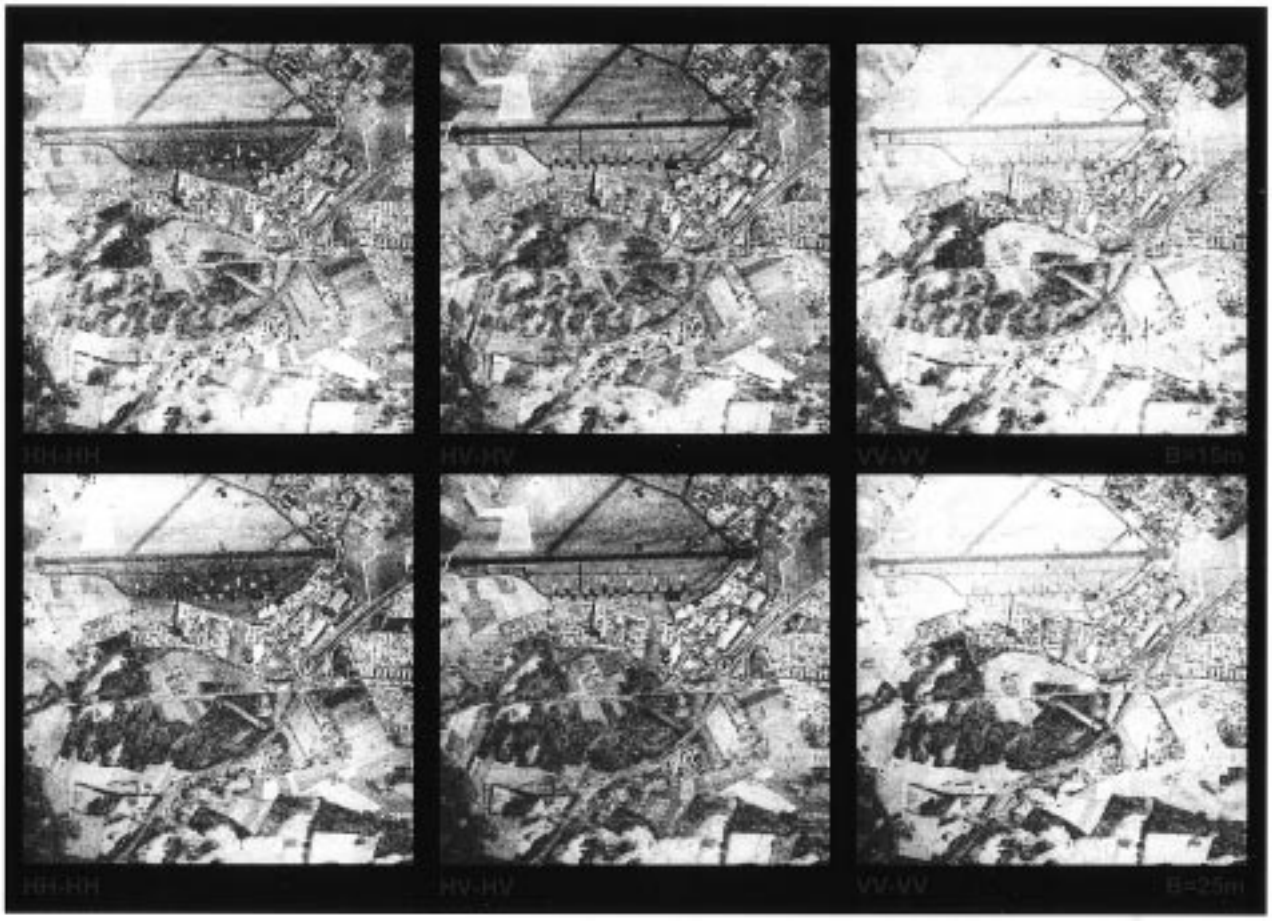

Fig. 4. Coherence maps of interferograms in the (H,V)-polarization basis for two baselines. (Top) $B = 15$ m, (bottom) $B = 25$ m, (left) $S_{1_{HH}} S^*_{2_{HH}}$, (middle) $S_{1_{HV}} S^*_{2_{HV}}$, abd (right) $S_{1_{VV}} S^*_{2_{VV}}$.

The only alternative scenario, apart from a random volume over a depolarising ground, which leads to three different coherence values in the three orthogonal polarizations is the presence of orientation effects in the volume. These have been considered in [14], [15]. In the following, we shall show that orientation effects are not relevant for forested areas at L-band.

Summarizing, in terms of the random volume over ground scattering model the variation of $\vec{w}$ implies a variation of the effective ground-to-volume amplitude ratios, mainly caused by the strong polarimetric behavior of the ground. Consequently, the variation of m leads to a variation of the location of the effective scattering center with polarization, and hence, the interferometric coherence becomes a function of polarization.

D. Optimum Polarizations

As discussed in the previous section, in the extreme case of zero ground contribution the interferometric coherence becomes independent of polarization. In this case, the coherence optimization algorithm performs a pure signal-to-noise optimization. All three optimum polarizations have the same scattering center, which location depends on the volume height and extinction. Assuming a sufficiently high SNR

$$|\tilde{\gamma}_1(\vec{w}_1)| = |\tilde{\gamma}_2(\vec{w}_1)| = |\tilde{\gamma}_3(\vec{w}_1)| = |\tilde{\gamma}_V| < 1. \qquad (18)$$

At the other extreme, where only ground scattering occurs, the scattering center for all polarizations is located on the ground and apart from SNR decorrelation effects

$$|\tilde{\gamma}_1(\vec{w}_1)| = |\tilde{\gamma}_2(\vec{w}_1)| = |\tilde{\gamma}_3(\vec{w}_1)| = 1 \qquad (19)$$

In general, the situation will lie between these two extremes. For the case of a random vegetation layer over a multicomponent ground scatterer, the coherence optimization algorithm is trying to select the ground that gives the inherently highest coherence. But in the case of a random volume of nonspherical particles, it is not possible to remove totally the coherence reducing volume contribution. In order to maximize the interferometric coherence, the algorithm compromises between maximizing the ground return and minimizing the volume contribution. Thus, it identifies as optimal the polarization in which the effective ground-to-volume amplitude ratio m is maximized. The second optimum coherence value corresponds to a ground-to-volume amplitude maximization performed in a two-dimensional (2-D) subspace orthogonal to the first solution. Finally the third optimum coherence value represents the maximization of m in the one-dimensional (1-D) subspace orthogonal to the first and second solutions. In the case of two orthogonal ground scattering components, (for example direct surface scattering and dihedral ground-trunk interaction) this third optimum coherence

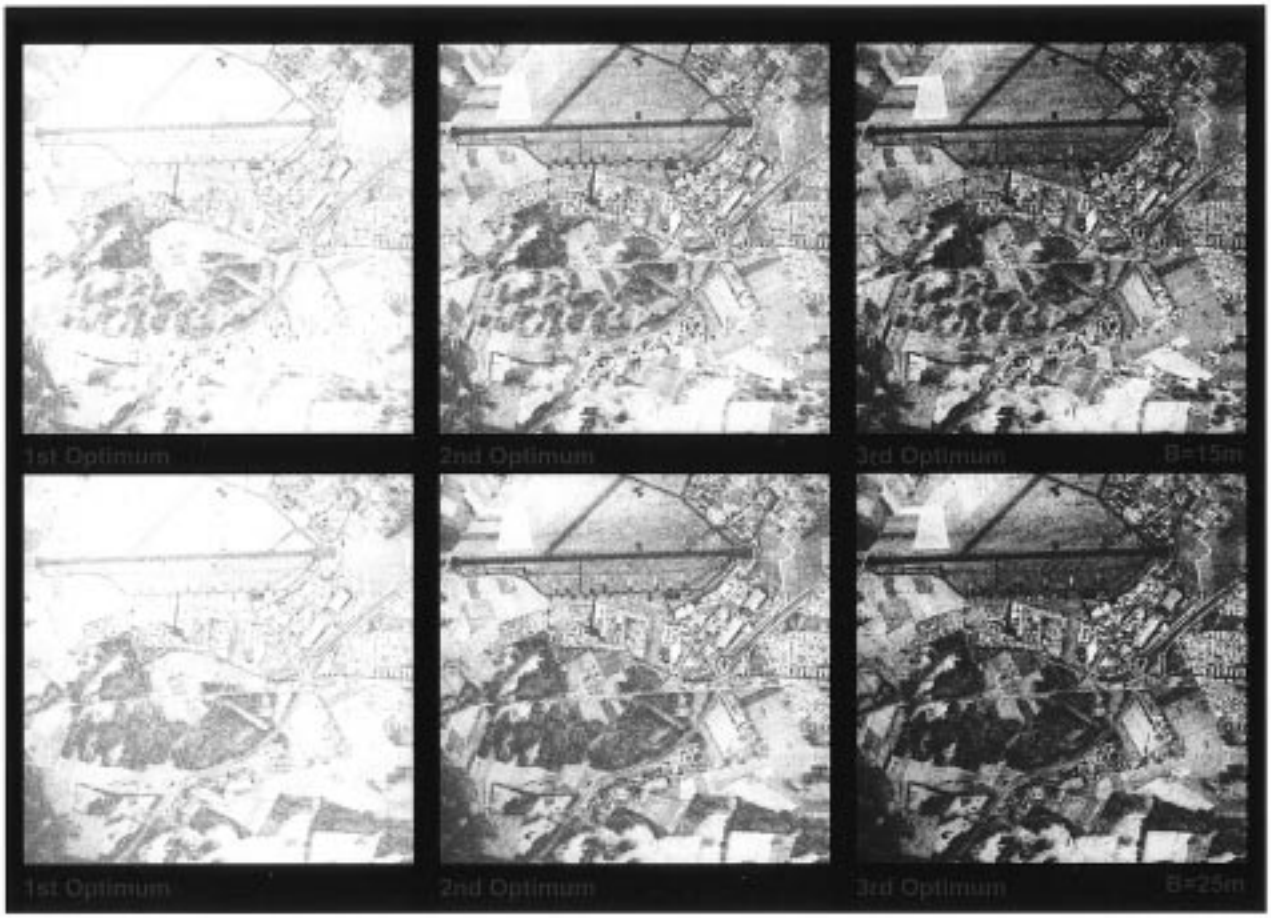

Fig. 5. Coherence maps of interferograms for two baselines. (Top) $B = 15$ m, (bottom) $B = 25$ m, generated by using the optimum scattering mechanisms related to the (left) first, (middle) second, and (right) third singular value.

value equals the volume coherence $\gamma_3 = |\tilde{\gamma}_V|$, since the ground components lie in the orthogonal subspace defined by the first two solutions. However, in the presence of a three-component ground, even the third optimum coherence value is affected by a ground scattering component which has to be accounted for. Thus, the optimization algorithm determines three different coherence values corresponding to different ground to volume amplitude ratios $m_1 > m_2 > m_3$

$$|\tilde{\gamma}_1(\vec{w}_1)| > |\tilde{\gamma}_2(\vec{w}_2)| > |\tilde{\gamma}_3(\vec{w}_3)|. \tag{20}$$

The location of the effective scattering center for each optimum scattering mechanism depends on the corresponding ground-to-volume amplitudes and the attenuation length in the volume. The residual volume component forces all three coherence values to be baseline dependent to a degree dependent on the amount of the individual ground component.

Fig. 5 shows the optimum coherence maps for the 15 m (top) and the 25 m baseline (bottom). As expected, the optimum coherence values becomes one on the fields but drops down in the forested areas because of the residual volume component, which cannot be removed. The first optimum coherence is for both baselines significantly higher than the conventional coherences shown in Fig. 4. At the same time, it shows the lowest baseline variation indicating a higher ground scattering component. On the other hand, the third optimum coherence is over the forested areas lower than the $S_{1_{HV}} S^*_{2_{HV}}$ indicating the presence of a cross-polarizing ground component. This underlines the assumption of a three-component ground as indicated in (17).

E. Geometrical Interpretation of the Scattering Model

The significance of any scattering model depends on its ability to fit experimental observations. Up to now, the efficiency of the random volume over ground model to interpret the experimental observations was demonstrated, as an indirect proof for the validity of the model. The key point for a direct validation of the model is to recognize that the only parameter in (12) which is a function of polarization is the ground-to-volume amplitude ratio m. This ratio depends on the choice of the unitary scattering mechanism $\vec{w}$. The real parameter m generates a straight line in the complex plane. This can be shown by rewriting (12) as

$$\tilde{\gamma}(\vec{w}) = \exp(i\phi_0)\left[\tilde{\gamma}_V + \frac{m(\vec{w})}{1+m(\vec{w})}(1-\tilde{\gamma}_V)\right]. \tag{21}$$

(21) represents the equation of a straight line in the complex plane going through the point $\tilde{\gamma}_V$ with direction $(1-\tilde{\gamma}_V)$. The model then has a geometrical interpretation as shown in Fig. 6. The solid line represents the extent of the observable coherence values with polarization. The length of this segment depends

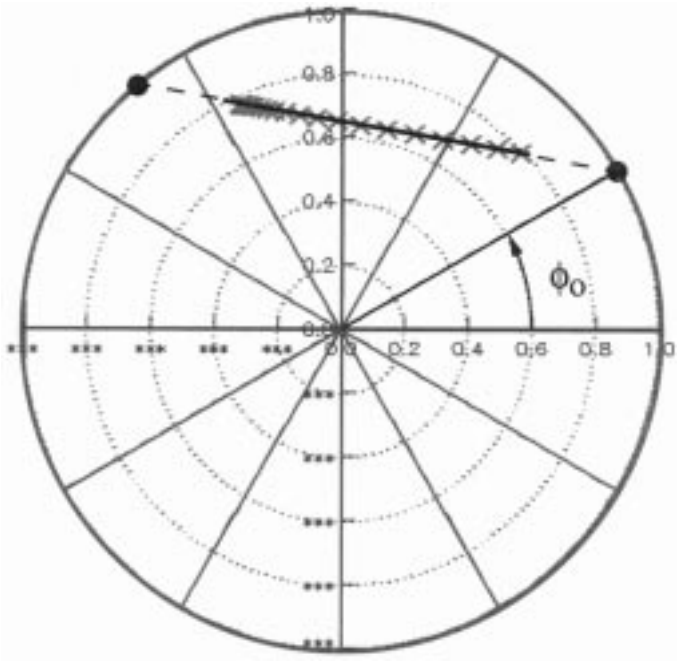

Fig. 6. Geometrical interpretation of polarimetric interferometry for the random volume over ground scattering model.

on the baseline, the radar frequency, the height and mean extinction of the vegetation layer and the amplitude of the ground scattering mechanisms [16], [17].

In order to determine if the linear model provides an accurate description of forest scattering at L-band, we check it against the experimental data. To obtain a distribution of coherence values with polarization, we use the $S_{1_{HH}}S^*_{2_{HH}}$, $S_{1_{HV}}S^*_{2_{HV}}$, and $S_{1_{VV}}S^*_{2_{VV}}$ coherences and augment these with the three optimum coherence values. Typical coherence signatures and the corresponding least squares fits for forested areas are shown in Figs. 7(a) and 7(c), while in Fig. 7(b), a typical surface scatterer coherence signature is presented. The locations of the test areas are marked in Fig. 3. The good linearity for the forest scatterers in the complex plane, as predicted from (22), again supports the assumption of the random volume over ground scattering model for the interpretation of fully polarimetric interferometric data over forested terrain at L-band. For the surface scatterer, (22) predicts the shrinking of the straight line into a point on the unit circle. However the variation of the of signal-to-noise decorrelation contributions with polarization leads to a radial line in the complex plane, indicating a change of coherence with polarization but common mean interferometric phase. Note that all three points have the same intersection point which indicates the same underlying topography, which is in accordance with the flat terrain of the test site [18].

IV. Parameter Estimation

Having validated the scattering model and examined the influence of polarization, we turn now to the problem of parameter estimation. As already mentioned in Section II, for a single-baseline single-polarization configuration, the inversion of the random volume over ground model leads to an underestimated problem with four unknowns and only two observables. According to (12), any additional polarimetric channel operating in a single baseline interferometric mode increases the number of observables by two, but at the same time introduces one additional unknown parameter: the ground-to-volume amplitude ratio for the new polarization. Consequently, the inversion of the random volume over a ground scattering scenario using a single baseline requires at least three independent polarizations, and therefore, fully polarimetric interferometric data.

With $\tilde{\gamma}_1$, $\tilde{\gamma}_2$, and, $\tilde{\gamma}_3$ defined as the three observed complex coherence values of interferograms formed using different polarizations, the inversion algorithm can by formulated as

$$\begin{bmatrix} h_V \\ \exp(i\phi_0) \\ \sigma \\ m_1 \\ m_2 \\ m_3 \end{bmatrix} = \left[\mathcal{M}\right]^{-1} \begin{bmatrix} \tilde{\gamma}_1 \\ \tilde{\gamma}_2 \\ \tilde{\gamma}_3 \end{bmatrix}. \tag{22}$$

The operator $\left[\mathcal{M}\right]$ represents the scattering model as given in (12)–(15), which relates the six measurables to the six physical parameters of the scattering process. As the unknown parameters are coupled, (22) becomes a six-dimensional (6-D) nonlinear parameter optimization problem

$$\min\left(\left\| \begin{bmatrix} \tilde{\gamma}_1 \\ \tilde{\gamma}_2 \\ \tilde{\gamma}_3 \end{bmatrix} - \left[M\right] \begin{bmatrix} h_V \\ \exp(i\phi_0) \\ \sigma \\ m_1 \\ m_2 \\ m_3 \end{bmatrix} \right\|\right) \tag{23}$$

where $\|\ldots\|$ indicates the Euclidean vector norm. Equation (23) can be implemented as indicated in Fig. 8. A set of candidate parameters (h_V, ϕ_0, σ, m_1, m_2, m_3) is transformed through the model $[\mathcal{M}]$(12)–(15) into a vector that contains the modeled observables $\vec{M} = [\tilde{\gamma}_{m1}, \tilde{\gamma}_{m2}, \tilde{\gamma}_{m3}]^T$. Then the distance $\|\vec{M}-\vec{O}\|$ between the modeled vector and the vector of the real observables $\vec{O} = [\tilde{\gamma}_1, \tilde{\gamma}_2, \tilde{\gamma}_3]^T$ is evaluated. If the distance is a minimum, then the candidate parameters are the solution of the inversion problem. If not, the candidate parameters are modified until they lead to a minimum distance constraining positive h_V, σ, and m_i values [19].

A. Conditioning and Uniqueness of the Estimation Problem

The performance of the inversion algorithm depends of course on the choice of the three selected polarizations. The key point for achieving high parameter estimation accuracy is a well conditioned inversion problem. Due to the different ground contributions, the effective scattering centers at the three selected polarizations $\tilde{\gamma}_1$, $\tilde{\gamma}_2$, and $\tilde{\gamma}_3$ are located at different heights (indicated with z_1, z_2 and z_3 in Fig. 1). The scattering centers can be estimated in terms of the interferometric phase within its standard deviation, which is a function of the interferometric coherence [20], [21]. For a well conditioned inversion problem, the separation of the effective scattering centers must be larger than the height uncertainty caused due to the corresponding phase standard deviations. In this sense, three polarizations with high interferometric coherences do not necessarily ensure good conditioning. In fact, polarizations

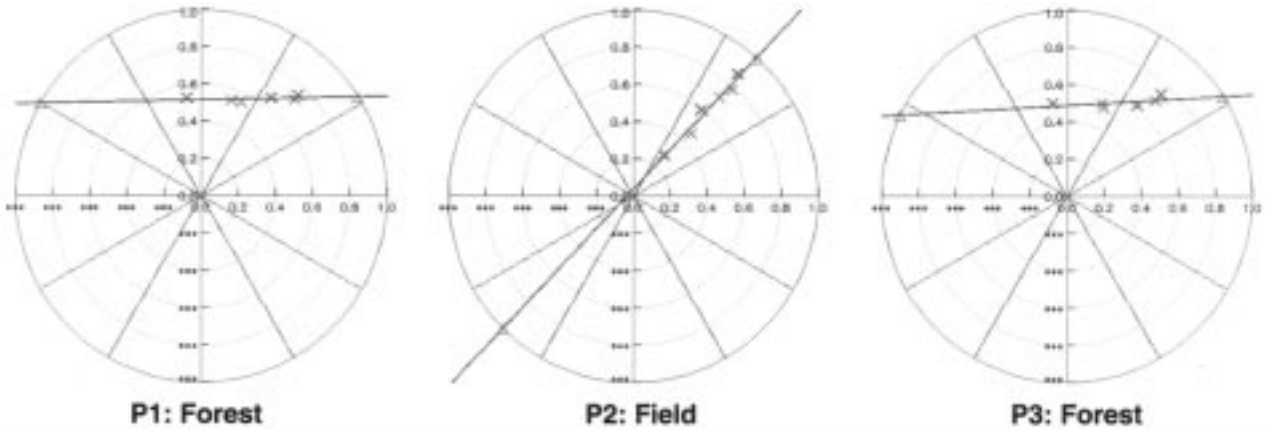

Fig. 7. Complex plane signatures of selected test areas: (a) forest scatter (marked as point P1 in Fig. 3), (b) surface scatter (point P2), and (c) forest scatter (point P3).

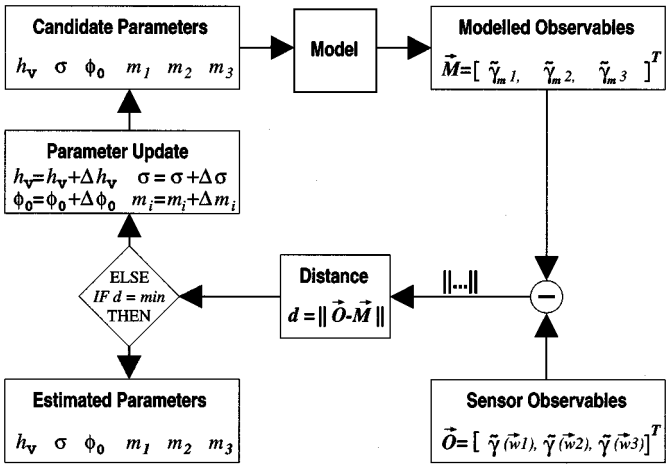

Fig. 8. Nonlinear inversion algorithm implementation scheme.

which combine distant scattering centers and yet maintain high coherences, which permit their scattering centers to be distinguishable, are required for a well conditioned inversion problem.

In the ideal case of three orthogonal scattering mechanisms (two on the ground and one in the vegetation layer), $m_1 = m_2 = \infty$, while $m_3 = 0$. The volume scattering is orthogonal to the ground scattering, and the inversion problem becomes decoupled. The observables are then directly related to single parameters. The interferometric phase of the first and second optimum polarizations represents the ground topography, while that of the third one represents the effective vegetation height. Thus in this case, the phase difference between the corresponding interferograms leads directly to the effective vegetation height, as suggested in [7]. However, this is unlikely to be the case in general and hence, a full nonlinear inversion must be applied.

The conventional polarizations S_{HH}, S_{HV}, and S_{VV} are likely to have separable phase centers and different coherences but the separation of their phase centers is not optimized. Therefore, their choice leads in general to a suboptimum inversion performance. On the other hand, the coherence optimization algorithm provides three independent scattering mechanisms that lead to the maximum possible interferometric coherences. These optimum polarizations are characterized by the widest possible ground-to-volume amplitude ratio spectrum optimized with respect to the interferometric coherence and therefore, the best possible separation of their phase centers. Hence, they lead to the best achievable conditioning of the inversion problem. Consequently, in the sense of parameter inversion, the coherence optimization algorithm may be interpreted as a data adaptive preconditioning procedure for the inversion algorithm.

Finally, to demonstrate the influence of the width of the ground-to-volume amplitude ratio spectrum of the selected polarizations on the conditioning of the inversion problem, we simulate the inversion performance for two different scenarios: a wide ground-to-volume amplitude spectrum with $m_1 : m_2 : m_3 = 1.0 : 0.1 : 0.01$ and for a narrow spectrum with $m_1 : m_2 : m_3 = 0.1 : 0.05 : 0.01$. The m values are referred to a volume height $h_V = 30$ m and an extinction coefficient $\sigma = 0.2$ dB/m for a vertical wavenumber $\kappa_z = 0.06$ (corresponding to a baseline of 15 m for the configuration used in Fig. 2). Using the scattering model, we evaluate the expected complex coherence values for seven different volume heights ranging from 5 up to 35 m, and perturb them with an amplitude standard deviation of 5% and a phase standard deviation according to the four-look statistics of the corresponding coherence values. Then we apply the inversion as addressed in (22). Fig. 9 shows on the top the results obtained for the first and on the bottom, the results for the second scenario. As one can see, the estimation accuracy for all parameters is significantly better for the wide ground spectrum. With increasing tree height, the estimation accuracy of h_V and ϕ decreases in both cases due to increasing volume decorrelation. The estimation of the extinction coefficient is inaccurate for short vegetation and improves with increasing tree height, as a minimum attenuation length is required in order to obtain sensitivity for σ.

The nonlinear problem in (23) has in general multiple solutions. In order to extract the true physical solution from the spurious ones, extra constraints must be applied. One problem can arise for long baselines when phase ambiguities in height can occur. This can be avoided by setting the ambiguous height well above the maximum expected tree height. A second problem arises with height/extinction ambiguities. This can be resolved

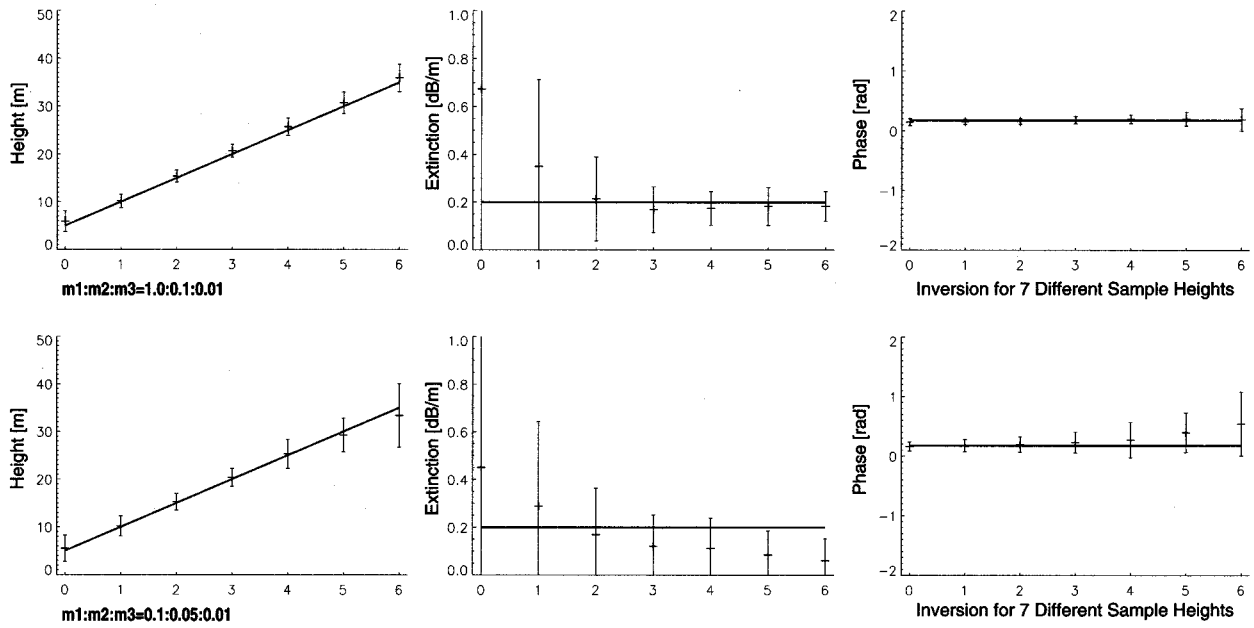

Fig. 9. Inversion performance for (top) a wide $m_1 : m_2 : m_3 = 1.0 : 0.1 : 0.01$ and (bottom) a narrow $m_1 : m_2 : m_3 = 0.1 : 0.05 : 0.01$ ground to volume amplitude spectrum. (Left) h_V estimation, (middle) σ estimation, and (right) ϕ_0 estimation.

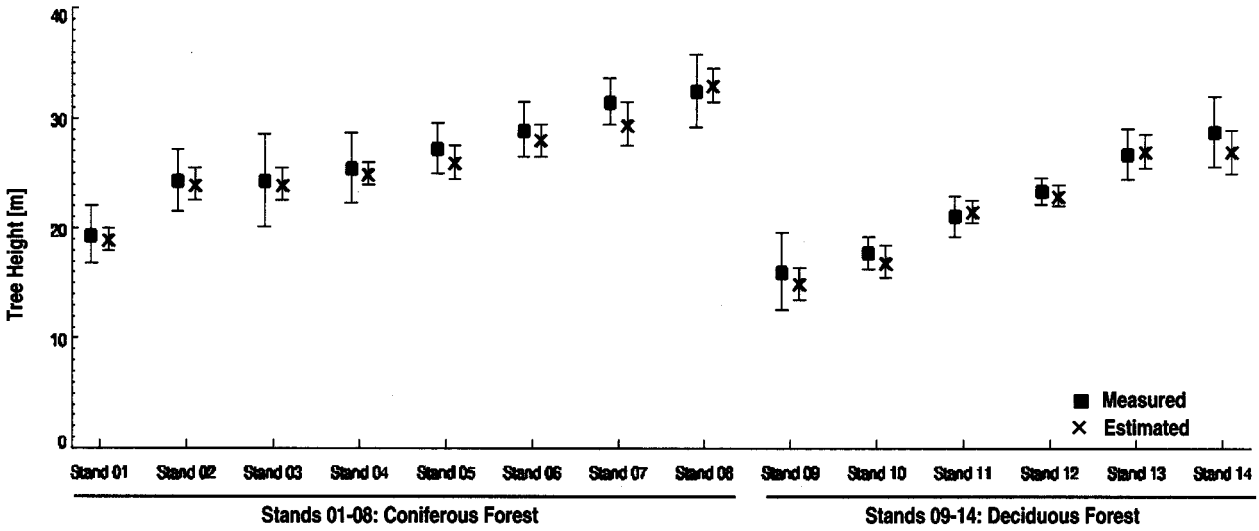

Fig. 10. Estimated ($\times$) and measured ($\square$) forest height for the 14 test stands.

by employing, as one of the triplet of coherences, a polarization channel with zero ground component. However, as mentioned above, there is no polarization channel, which can be considered to have a zero ground scattering component. Therefore, it is of importance to ensure minimization of the ground to volume ratio employing the optimum polarization channels as the cross-polarized channel does not necessarily minimize the ground component. By doing this, we can keep the height/extinction ambiguities tightly localized around the true values, as we demonstrate in simulations in Fig. 9 and in real data in Fig. 10.

B. Experimental Results

In order to validate the performance of the inversion algorithm, eight coniferous (Stands 1–8) and five deciduous (Stands 9–14) homogeneous forest stands, with heights ranging from 15 m up to 35 m, were selected. The locations of the stands are marked in Fig. 3. For these stands, the inversion algorithm was applied using the optimum polarizations for the 15 m baseline data. Because of the long baseline ($\kappa_z \approx 0.3$ in near-range), a phase multilooking by using a 7×7 window was performed to reduce the interferometric phase variation. Fig. 10 shows the estimated compared to the measured tree heights for all 14 stands. The mean values of the measured heights, averaged over each individual stand, are indicated with squares while the crosses indicate the corresponding mean values of the estimated heights. The error bars represents the height variation of each stand. As one can see, a good performance over the full range of heights for the coniferous as well as for the deciduous stands is achieved. The standard deviation between measured and estimated heights is about 2.5 m. Note that due to the strong phase

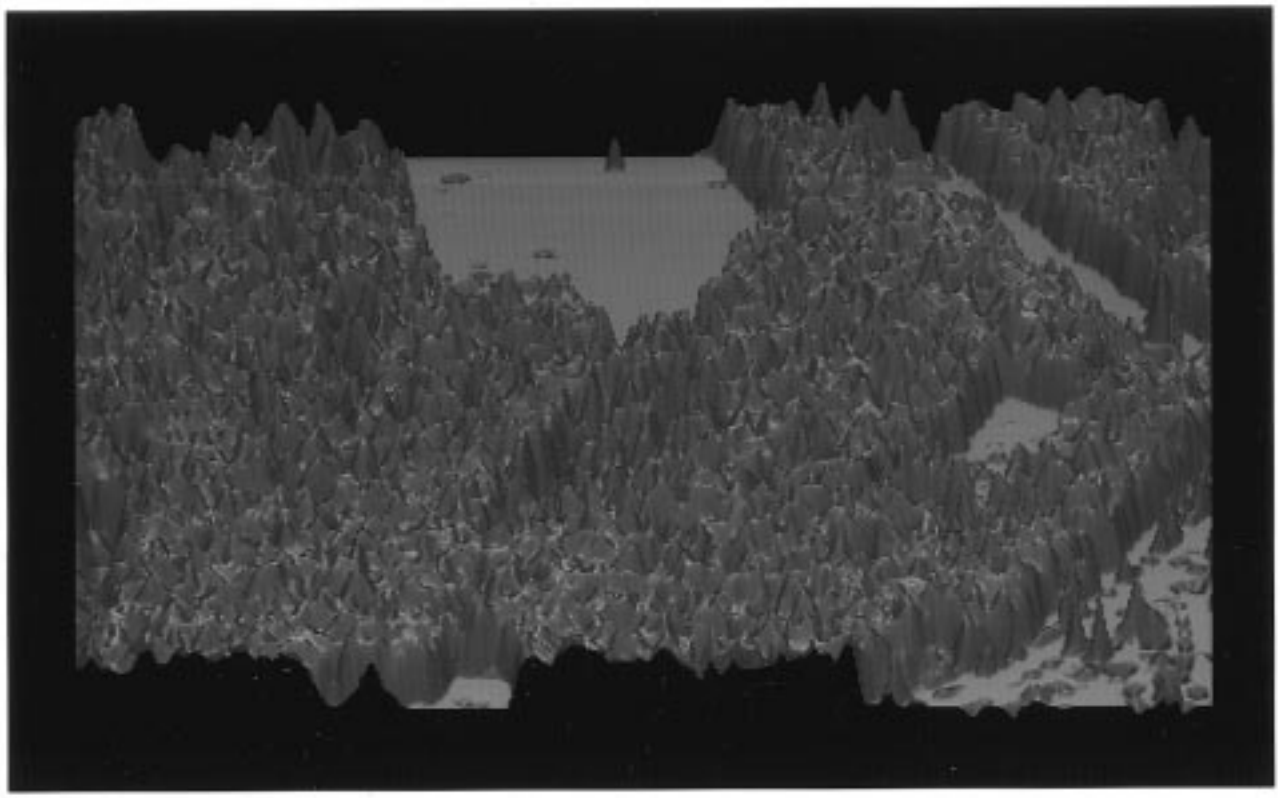

Fig. 11. Three-dimensional perspective view of estimated forest height for the forested area boxed in Fig. 3.

multilooking the variation of the estimated heights is significantly smaller than the variation of the measured ones. The inversion of the second 25 m baseline data leads to similar results (less than 2 m standard variation between the two independent estimations) verifying the consistency of the proposed algorithm in terms of a second independent observation.

Fig. 11 shows a 3-D perspective view of the estimated forest height for the whole scene. The mean forest heights are of the order of 20–30 m and the mean extinction is about 0.2 dB/m in the forested areas. The height variation over homogeneous forest areas is about 1–3 m. The lack of high resolution area-wide ground data makes a large scale validation difficult. However, the extracted forest height results are in accordance with area-wide results obtained in the frame of a tomographic SAR experiment [13].

One of the advantages of the proposed inversion is that, as the case of surface scattering is included in the model as a limiting case, there is no need in general for pre-processing the data for the identification of the forested areas. The inversion algorithm is flexible enough to handle transitions from forested to open terrain. The only case where special attention must be given, is the case of smooth surface scatterers with low backscatter intensity. Because of signal noise induced decorrelation, these fields show a similar coherence behavior $1 > \gamma_1 \gg \gamma_2 \approx \gamma_3$ as sparse or low altitude forest areas.

V. Discussion and Conclusions

One of the central conclusions from the analysis of experimental data is the presence of both volume and ground scattering contributions in all polarizations. Therefore, a straightforward estimation of forest height in terms of the phase difference of scattering centers at different polarizations is in general not possible. A more sophisticated model-based inversion technique is necessary.

The fundamental importance of ground scattering is a second important conclusion of this work. On the one hand, any ground scattering component affects strongly the interferometric coherence. This makes the parameter inversion from interferometric observables not possible without an accurate estimation of the amount of ground scattering. On the other hand, the appearance of the ground forces the interferometric coherence to be polarization dependent. As polarimetry can be used, directly or indirectly, for the estimation of the ground scattering component, polarimetric interferometry becomes an important technique for vegetation parameter estimation.

The random volume over ground scattering model, despite its simplicity, seems to have enough physical structure for the interpretation of the experimental data sets in L-band. This is important because it allows the inversion of forest parameters from single baseline polarimetric interferometric data. A more extended vegetation scattering model would introduce additional parameters which can no longer be estimated without the need for *a priori* information or assumptions. One obvious way to overcome such problems is to extend the observation vector. Note that multifrequency single-baseline configurations are not able to provide an alternative. As two model parameters, the effective ground-to-volume amplitude ratio m and the volume extinction coefficient σ are frequency dependent, every additional frequency introduces the same number of unknowns as new ob-

servables. In contrary, dual or multibaseline single-channel configurations provide a potential solution of the random volume over ground scattering problem based on the dependency of $\tilde{\gamma}$ on κ_z, which changes with baseline [4], [5].

In this paper, we proposed an inversion algorithm based on single frequency, fully polarimetric, single baseline configuration. Using the interferometric coherence and phase information in three different polarizations we are able to estimate forest height, average forest extinction, and, underlying topography. The underlying topography can be used directly for mapping applications, while forest height is the most important single parameter for stem biomass estimation [22]. The extinction coefficient that is related to canopy density can be used potentially as an input parameter for a canopy biomass estimation model. Finally, the three ground to volume amplitude ratios allow for the first time the extraction of information about surfaces under dense vegetation cover. The proposed algorithm represents an important generalization of the results presented in [7].

Further, we proposed the use of the optimum polarizations for the solution of the inversion problem. The advantage of using the coherence optimization algorithm is that it provides an adaptive choice of polarizations which leads to the best possible conditioning of the problem independent on scatterers and/or topographic variations in the scene. This way, the highest parameter estimation accuracy can be achieved.

However, the inversion of the scattering model consumes all six available observables. There is no more remaining information that will allow the consideration of a more complicated vegetation structure. Therefore, any extension of the scattering model requires either the use of *a priori* information or more observables, as, for example, by using one or more additional baselines. The challenge to estimate a larger number of physical parameters is not the only reason for increasing the number of observations. The scattering model as addressed up to now does not consider any temporal effects. This is an essential limiting factor for wide application, especially for polarimetric spaceborne systems with their typical long temporal baselines. A more general inversion scenario including temporal decorrelation effects, which allows a more general application of the inversion algorithm with respect to repeat pass air and future spaceborne sensors as ALOS is discussed in [23] and [24].

ACKNOWLEDGMENT

The authors would like to thank R. Treuhaft, JPL, Pasadena, CA, A. Reigber, German Aerospace Center (DLR), Oberpfaffenhofen, Germany, and W-M. Boerner, University of Illinois, Chicago (UIC), for many constructive discussions and comments. They would also like to thank T. Boerner, DLR, for providing the tree height measurements.

REFERENCES

[1] R. Bamler and P. Hartl, "Synthetic aperture radar interferometry," *Inv. Probl.*, vol. 14, pp. R1–R54, 1998.

[2] J. O. Hagberg, L. M. Ulander, and J. Askne, "Repeat-pass interferometry over forested terrain," *IEEE Trans. Geosci. Remote Sensing*, vol. 33, pp. 331–340, Mar. 1995.

[3] J. Askne, P. B. Dammert, L. M. Ulander, and G. Smith, "C-band repeat-pass interferometric SAR observations of the forest," *IEEE Trans. Geosci. Remote Sensing*, vol. 35, pp. 25–35, Jan. 1997.

[4] R. N. Treuhaft, S. N. Madsen, M. Moghaddam, and J. J. van Zyl, "Vegetation characteristics and underlying topography from interferometric data," *Radio Sci.*, vol. 31, pp. 1449–1495, 1996.

[5] R. N. Treuhaft and P. R. Siqueira, "The vertical structure of vegetated land surfaces from interferometric and polarimetric radar," *Radio Sci.*, vol. 35, no. 1, pp. 141–177, 2000.

[6] W. M. Boerner *et al.*, "Polarimetry in radar remote sensing: basic and applied concepts," in *Manual of Remote Sensing*, R. Reyerson *et al.*, Ed. New York: Wiley, 1998, vol. 2, Principles and Applications of Imaging Radar, ch. 5.

[7] S. R. Cloude and K. P. Papathanassiou, "Polarimetric SAR interferometry," *IEEE Trans. Geosci. Remote Sensing*, vol. 36, pp. 1551–1565, Sept. 1998.

[8] K. P. Papathanassiou, S. R. Cloude, and A. Reigber, "Estimation of vegetation parameters using polarimetric SAR interferometry part i and ii," in *Proc. CEOS SAR Worhshop 1999 CNES*, Toulouse, France, Oct. 26–29, 1999.

[9] A. Reigber, K. P. Papathanassiou, S. R. Cloude, and A. Moreira, "SAR tomography and interferometry for the remote sensing of forested terrain," in *Proc. 3rd Eur. Conf. Synthetic Aperture Radar EUSAR 2000*, Munich, Germany, May 23–25, 2000, pp. 137–140.

[10] S. R. Cloude, J. Fortuny, J. M. Lopez, and A. J. Sieber, "Wide band polarimetric radar inversion studies for vegetation layers," *IEEE Trans. Geosci. Remote Sensing*, vol. 37, pp. 2430–2442, Sept. 1999.

[11] S. R. Cloude, I. Hajnsek, and K. P. Papathanassiou, "Eigenvector methods for the extraction of surface parameters in polarimetric SAR," in *Proc. CEOS SAR Workshop*, Toulouse, France, Oct. 26–29, 1999.

[12] I. Hajnsek, S. R. Cloude, J. S. Lee, and E. Pottier, "Inversion of surface parameters from polarimetric SAR," in *Proc. IGARSS'00*, Honolulu, HI, July 24–28, 2000, pp. 1095–1097.

[13] A. Reigber and A. Moreira, "First demonstration of airborne SAR tomography using multibaseline L-band data," *IEEE Trans. Geosci. Remote Sensing*, vol. 38, pp. 2142–2152, Sept. 2000.

[14] R. N. Treuhaft and S. R. Cloude, "The structure of oriented vegetation from polarimetric interferometry," *IEEE Trans. Geosci. Remote Sensing*, vol. 37, pp. 2620–2625, Sept. 1999.

[15] S. R. Cloude, K. P. Papathanassiou, and W. M. Boerner, "The remote sensing of oriented volume scattering using polarimetric radar interferometry," in *Proc. Int. Symp. Antennas and Propagation, ISAP'00*, Fukuoka, Japan, Aug. 22–25, 2000.

[16] S. R. Cloude, K. P. Papathanassiou, and A. Reigber, "Polarimetric SAR interferometry at P-band for vegetation surface extraction," in *Proc. 3rd Eur. Conf. Synthetic Aperture Radar EUSAR 2000*, Munich, Germany, May 23–25, 2000, pp. 249–252.

[17] S. R. Cloude, K. P. Papathanassiou, A. Reigber, and W. M. Boerner, "Multi-frequency polarimetric SAR interferometry for vegetation structure extraction," in *Proc. IGARSS'00*, Honolulu, HI, July 24–28, 2000.

[18] S. R. Cloude, K. P. Papathanassiou, and W. M. Boerner, "A fast method for vegetation correction in topographic mapping using polarimetric radar interferometry," in *Proc. 3rd Eur. Conf. Synthetic Aperture Radar EUSAR 2000*, Munich, Germany, May 23–25, 2000, pp. 261–264.

[19] W. H. Press, S. A. Teukolsky, W. T. Vettering, and B. P. Flannery, *Numerical Recipies in Fortran*, 2nd ed. Cambridge, U.K.: Cambridge Univ. Press, 1992.

[20] D. Just and R. Bamler, "Phase statistics of interferograms with applications to synthetic aperture radar," *Appl. Opt.*, vol. 33, no. 20, pp. 4361–4368, July 1994.

[21] J. S. Lee, K. P. Papathanassiou, T. Ainsworth, M. R. Grunes, and A. Reigber, "A new technique for noise filtering of SAR interferometric phase images," *IEEE Trans. Geosci. Remote Sensing*, vol. 36, pp. 1456–1465, Sept. 1998.

[22] M. Moghaddam and J. L. Dungan, "Fusion of SAR and TM data for quantitative estimation of forest variables over an extended range of validity," in *Proc. IGARSS'00*, Honolulu, HI, July 24–28, 2000, pp. 954–956.

[23] K. P. Papathanassiou, S. R. Cloude, and A. Reigber, "Single and multibaseline polarimetric SAR interferometry over forested terrain," in *Proc. 3rd Eur. Conf. Synthetic Aperture Radar EUSAR 2000*, Munich, Germany, May 23–25, 2000, pp. 123–126.

[24] K. P. Papathanassiou, S. R. Cloude, A. Reigber, and W. M. Boerner, "Multi-baseline polarimetric SAR interferometry for vegetation parameters extraction," in *Proc. IGARSS'00*, Honolulu, HI, July 24–28, 2000.

Konstantinos P. Papathanassiou received the Dipl.Ing degree and the Dr. degree from the Technical University of Graz, Graz, Austria, in 1994 and 1999, respectively.

From 1992 to 1994, he was with the Institute for Digital Image Processing (DIBAG), Joanneum Research, Graz. From 1995 to 1999, he was a Scientist with the Institute for Radio Frequency Technology (HF) of the German Aerospace Center (DLR), Wessling, Germany. From 1999 to 2000, he was with Applied Electromagnetics (AEL), St. Andrews, U.K., in the frame of the EC-TMR Radar Polarimetry Network. In October 2000, he again joined the Institute for Radio Frequency Technology, DLR, working on polarimetric and interferometric processing techniques, modeling of natural scattering processes, and the development of inversion algorithms for physical parameters from SAR data.

His main research interests are in electromagnetic propagation and scattering theory, radar polarimetry, SAR, and interferometric SAR data processing techniques. He has more than 40 publications in international journals, conferences, and workshops. In 1998, he was awarded the IEEE IGARSS Symposium Prize Paper Award.

Shane R. Cloude received the B.Sc. degree from the University of Dundee, Dundee, U.K., in 1981, and the Ph.D. degree from the University of Birmingham, Birmingham, U.K., in 1987.

He was a Radar Scientist with the Royal Signals and Radar Establishment, Great Malvern, U.K. Following this, he held teaching and research posts at the University of Dundee, Dundee, U.K. the University of York, York, U.K., and the University of Nantes, Nantes, France, before taking on his present role in 1996. He is now a Senior Scientist with AEL Consultants, undertaking research on a range of problems associated with radar and electromagnetic scattering. His research interests are in polarization effects in electromagnetic scattering and their applications in radar and optical remote sensing. He is the author of ten book chapters, 18 journal publications, and over 50 international conference and workshop papers.

Dr Cloude is a Fellow of the IEEE Geoscience and Remote Sensing Society, a Fellow of the Alexander von Humboldt Foundation in Germany, and Honorary Professor at the University of Dundee.